Carbohydrate Polymer Technologies and Applications 6 (2023) 100382

Contents lists available at ScienceDirect

Carbohydrate Polymer Technologies and Applications

journal homepage: www.sciencedirect.com/journal/carbohydrate-polymer-technologies-and-applications

Visible light-mediated cross-linking of injectable gellan gum hydrogels embedding human chondrocytes

Diego Trucco [a,b,c,*,1], Lorenzo Vannozzi [a,b,1], Elena Gabusi [c], Enrico Lenzi [c], Cristina Manferdini [c], Alessia Bacci [a,b], Liliana Agresti [a,b], Maria Rosaria Pascale [d], Sandra Cristino [d], Gina Lisignoli [c], Leonardo Ricotti [a,b]

[a] The BioRobotics Institute, Scuola Superiore Sant'Anna, Piazza Martiri della Libertà 33, Pisa 56127, Italy
[b] Department of Excellence in Robotics & AI, Scuola Superiore Sant'Anna, Piazza Martiri della Libertà 33, Pisa 56127, Italy
[c] IRCCS Istituto Ortopedico Rizzoli, SC Laboratorio di Immunoreumatologia e Rigenerazione Tissutale, Via di Barbiano, 1/10, Bologna 40136, Italy
[d] Department of Biological, Geological, and Environmental Sciences, University of Bologna, Via San Giacomo 12, Bologna 40126, Italy

ARTICLE INFO

Keywords:
Methacrylated gellan gum
Natural polymer
Visible light
Photo-crosslinking optimization
Steam sterilization
Chondrocytes

ABSTRACT

Gellan gum, a polysaccharide with structural similarities to glycosaminoglycans, is gaining attention in cartilage tissue engineering. It can be chemically modified with methacrylic moieties to produce a photo-crosslinkable formulation, called methacrylated gellan gum (GGMA), envisaging the injection and the in situ cross-linking through light on the cartilage surface.

This study aimed to investigate the visible light cross-linking of GGMA, underlying the impact of steam sterilization on its chemical and rheological properties and cross-linking efficiency. After an initial assessment of the sterilization effects, we evaluated a combination of hydrogel concentrations (1 and 2 % w/v), ruthenium/sodium persulfate concentrations (0.1/1, 0.2/2 and 0.5/5 mM ratios), and light exposure times (30, 60 and, 120 s). The formulations with the lowest sol fraction were characterized for mechanical and showed self-healing properties. Biological characterization on encapsulated chondrocytes in hydrogels showed high cell viability with increased metabolic activity over two weeks. The expression of genes encoding collagen type II and cartilage oligomeric matrix protein was upregulated in the softer formulation ($E = 0.95 \pm 0.48$ kPa) composed of 2 % w/v GGMA, 0.1/1 mM Ru/SPS, and photo-crosslinked for 60 s. These findings represent an interesting overview of the potential application of visible-light crosslinked GGMA in the clinical scenario to treat cartilage defects.

1. Introduction

Articular cartilage has a minimal ability to heal for the lack of a vascular network, making the repair of a defect challenging for the body (Huang et al., 2022). The loss of cartilaginous tissues may occur due to pathological conditions such as osteoarthritis or traumas, including intra-articular fracture and ligament injury. While injuries can be partially self-regenerated when the defect diameter is less than 3 mm (even if the appearance of the fibrocartilage is the most common condition), a diameter higher than 4 mm makes self-repairability inefficient (Asadi et al., 2018). Currently, orthopaedic surgeons perform mosaicplasty, microfracture and autologous chondrocytes or stem cell injection for the larger lesions, with a relative success rate (Arshi, Petrigliano, Williams, & Jones, 2020; Chimutengwende-Gordon, Donaldson, & Bentley, 2020; Wang, Yuan, Guo, Lu, & Peng, 2015). However, the common limitation that still affects such treatments is the inability to avoid the predominant formation of fibrocartilage (mostly made of collagen type I), which may severely impair the biomechanical performance of the newly formed cartilage with respect to the native one, causing potential clinical issues for the patients in the long-term (Armiento, Alini, & Stoddart, 2019). For this scope, the development of new strategies to efficiently restore cartilage function and avoid or delay total joint replacement is crucial.

In this perspective, cartilage tissue engineering (CTE) aims at restoring the native tissue using cells and scaffolds to replace the defective cartilage. Scaffolds can support cell growth and the production

* Corresponding author.
E-mail address: diego.trucco@santannapisa.it (D. Trucco).
[1] D.T. and L.V. contributed equally to this work.

https://doi.org/10.1016/j.carpta.2023.100382

Available online 21 October 2023

of new extracellular matrix (ECM) by the cells and, in the meantime, degrade to leave room for the development of the newly engineered biological tissue (Kwon et al., 2019). Amongst scaffolds, hydrogels have emerged as attractive ones due to their biocompatibility and ability to resemble the tissue ECM (Wei et al., 2021). In particular, cell-laden injectable hydrogels have the potential to overcoming the limitations of the current surgical treatments: they can be injected locally in the site of interest, and conform to its shape.

In recent years, gellan gum (GG) attracted the interest of several research groups in this field, due to its structural similarity with native articular cartilage glycosaminoglycans due to the presence of glucuronic acid residues (Oliveira et al., 2010, 2010). GG is an anionic linear polysaccharide produced by the bacterium *Sphingomonas elodea*, that rapidly cross-links after interacting with monovalent and divalent ions (Coutinho et al., 2010; Zhang, Xu, Qu, Xi, & Yang, 2014). GG-based hydrogels have several advantages over other hydrogels, including shear-thinning properties and gel formation at physiological temperatures, which favour its use as an injectable material (Oliveira et al., 2010). Indeed, in recent years, several approaches have been investigated to tune the GG features and increase its mechanical properties. Different cross-linking strategies have been devised, modifying the GG structure (Kim et al., 2019; Learmonth et al., 2020; Lee et al., 2020). For example, Tyramine-modified gellan gum (Ty-GG) hydrogels have been developed via horseradish peroxidase cross-linking, providing them with higher mechanical strength and resistance (Oliveira et al., 2021). Alternatively, GG hydrogels were functionalized with divinyl sulfone through Michael-type addition to offer higher strength to the polymeric network (da Silva et al., 2018). The development of photoresponsive GG represents an exciting strategy to form mechanically-tuneable matrices for safely hosting cells, controlling the cross-linking timing. This approach can overcome the issues related to ionically cross-linked matrices, which are hardly tuneable and have poor stability (i.e., weight loss, water uptake, cross-linking stability, and mechanical properties) in physiological environments (Silva-Correia et al., 2013; Su, Chen, & Lin, 2010).

Several studies focused on GG methacrylation for producing methacrylated gellan gum (GGMA), to tune the cross-linking degree of the polymer by combining physical and chemical cross-linking methods (Bacelar, Silva-Correia, Oliveira, & Reis, 2016; Xu, Li, Jiang, & Bratlie, 2018). Also, GGMA is water-soluble at room temperature and easily usable as an injectable biomaterial unlike GG, which injectability is restricted to a small temperature window, making it more challenging to be implemented clinically. The photo-crosslinking technique applied to GGMA is not new. Silva-Correia and colleagues crosslinked GGMA using a UV lamp emitting light at 366 nm for a duration of 6 min, followed by stabilization in a phosphate buffer saline solution with a pH of 7.4 for 30 min. Their approach involved embedding fibroblasts for intervertebral disc regeneration (Silva-Correia et al., 2013). It is worth noting that Vilela et al. conducted a noteworthy study where they demonstrated the promising performance of cell-laden hydrogels composed of GG or GGMA, crosslinked solely using culture media without specifying the duration (Vilela et al., 2018). This research served as a preliminary proof of concept, highlighting GGMA's potential in cartilage regeneration both in Vitro and in Vivo. However, similar to previous studies of that group, their approach regarded just an ionically crosslinking without using UV or visible light.

Recently, GGMA was adjuvated with Manuka honey to make it printable and chondrogenic (Scalzone et al., 2022) or with κ-carrageenan to serve as a cartilage substitute (Kanca & Özkahraman, 2023). Another recent study exploited a blend with hyaluronic acid for image-guided interventions (Vieira et al., 2020). Alternatively, the GGMA has been mixed with methacrylated gelatine to make the mixture modifiable from the viscoelastic point of view for promoting fibroblast differentiation (Xu, Zhang, Bentil, & Bratlie, 2021). In these studies, the authors always used a UV light source to cross-link the material. However, the real usability of UV light in Vivo is still a matter of debate since radicals generated by photoinitiators under UV light can induce considerable damages to the cells (Cadet, Sage, & Douki, 2005). Indeed, the photoinitiator mixed within the hydrogel forms free radicals upon light exposure to bound polymer chains. At the same time, these molecules can lead to DNA damage and cell death as cytotoxic and genotoxic causes (Lee et al., 2020).

Unlike UV light, visible light-sensitive photoinitiators allow the cross-linking of photosensitive hydrogels through visible light, thus avoiding the possible side effects of UV. In this context, several photoinitiators have been recently proposed (Zheng et al., 2021). Type II photoinitiators based on Ruthenium (Ru) and sodium persulfate (SPS) represent the most studied ones, also for alleviating the effects of oxygen inhibition on the constructs, which compromise the complete cross-linking of hydrogels (Lim et al., 2019). Apart from a preliminary study focused on the comparative adhesive properties between GG and GGMA from our group (Trucco et al., 2022), visible light-mediated cross-linking of GGMA has never been systematically investigated in terms of physico-chemical property change after undergoing sterilization, so far. Furthermore, recent studies focused on photosensitive GGMA exploiting a cross-linking time higher than 3 min. A reduction of the cross-linking time would be beneficial for facilitating future clinical translation. Additionally, we propose this analysis evaluating a sterilized version of GGMA applying an autoclave treatment to the polymer powder, a rather underinvestigated aspect. Indeed, it is important to verify the effects of the sterilization procedure in the early phase of biomaterial development, since it may affect several properties, such as mechanical properties, biodegradation, bioactivity and printability (Rizwan, Chan, Comeau, Willett, & Yim, 2020).

In this work, we first evaluated the differences in terms of chemical properties between the non-sterilized and the autoclaved GGMA powder, and the potential alterations induced by such a treatment on the GGMA rheological properties. Then, visible light-mediated cross-linking was investigated under different photo-crosslinking conditions (polymer and photoinitiator concentration and visible light exposure time) to identify the hydrogels with the lowest sol fraction. Then, a few selected formulations were characterized in terms of mechanical and self-healing properties. Finally, human chondrocytes were embedded in these formulations and characterized in terms of viability and expression of collagen type II and cartilage oligomeric matrix protein, key markers of the articular cartilage tissue.

2. Material and methods

2.1. Materials

Gellan gum (GG, trademarked as GelzanCM), methacrylic anhydride (MA, degree of purity: > 94 %), phosphate-buffered saline without Ca^{2+}/Mg^{2+} (PBS), tris(2,2′-bipyridyl) ruthenium (II) chloride hexahydrate (Ru, 99.95 % trace metals basis), and SPS (degree of purity: > 98 %) were purchased from Merck (USA). Reagents were used without further purification. Dialyzing membranes (MWCO 12–14 kDa) were purchased from CelluSep (USA). CellCrown™ 24 well plate inserts were purchased from Scaffdex (Finland). FITC-conjugate albumin from bovine serum (BSA-FITC) was purchased from Invitrogen (ThermoFisher Scientific, USA). For the biological characterization human chondrocytes (cod. 402–05a) and their culture growth medium (HC Growth Medium, cod. 411–500) were purchased from Cell applications, Inc. (USA). Live/Dead (L/D) kit was purchased from Life Technologies (ThermoFisher Scientific, USA). PrestoBlue kit and TRizol reagent were purchased from Invitrogen (ThermoFisher Scientific, USA).

2.2. GGMA preparation

The methacrylation procedure was performed similarly to (Coutinho et al., 2010) and the same procedure reported in our previous work (Trucco et al., 2022). Briefly, GG was dissolved in deionized water

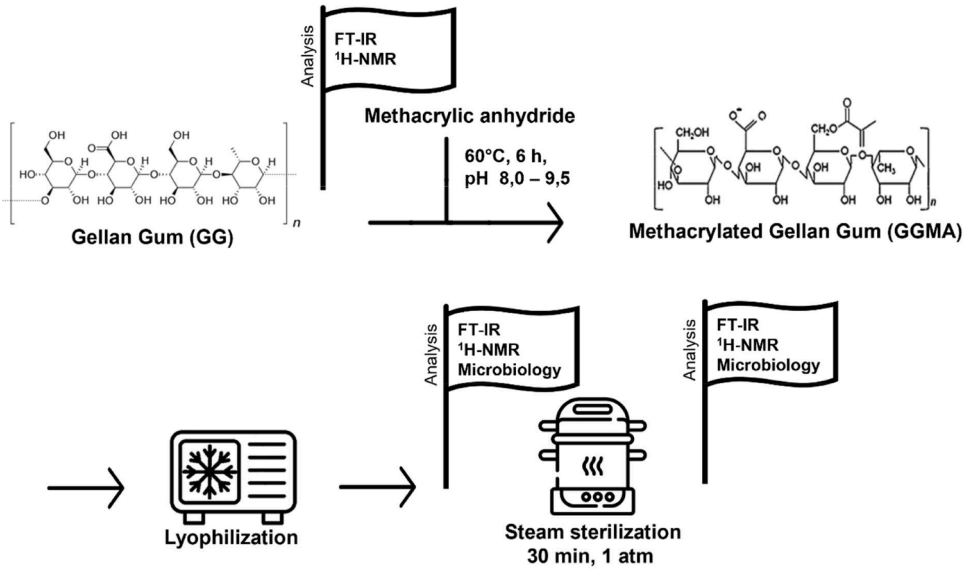

Fig. 1. Schematic representation of the procedure to obtain the steam-sterilized GGMA powder from GG; the flags represent the analyses performed on the material (FT-IR, ^{1}HNMR and microbiological analyses to verify material sterility).

(d-H_2O, 1 % w/v) with a magnetic stirrer at 75 °C for 1 h Then, the solution was cooled to 60 °C, and 8.5 mL of MA per 100 mL of solution was slowly added. The solution reacted for 6 h at a controlled pH range (8–9), then was centrifuged (3500 rpm for 3 min) at 30 °C to remove the unreacted MA, and the supernatant was diluted (1:2) with deionized water pre-heated at 40 °C. The solution was dialyzed at 60 °C for 5 d, quickly frozen and stored at −80 °C. Finally, aliquots were lyophilized (Labconco, FreeZone 2.5 Plus) for 3 days to obtain the methacrylated gellan gum (GGMA) powder and kept at −80 °C before use. The GGMA powder was also autoclaved at a temperature of 121 °C and a pressure of 1 bar for 30 min. A schematic representation of the GGMA preparation process and the subsequent analyses is shown in Fig. 1.

2.3. GGMA characterization

2.3.1. FT-IR and ^{1}HNMR

FT-IR spectra were recorded in attenuated total reflection (ATR) mode on GG (Gelzan^{CM}), on GGMA powder obtained thought the methacrylation procedure (GGMA) and after the steam sterilization with autoclave (Steam-sterilized GGMA), using an IRAffinity-1 FT-IR spectrophotometer equipped with an ATR MIRacle-10 accessory (Shimadzu Scientific Instrument, Japan) as depicted in Fig. 1. The spectra were recorded in the range 4000 – 600 cm^{-1}, setting 64 scans and a resolution of 4 cm^{-1}.

The ^{1}HNMR spectra (Bruker Ascend 400, Germany) were collected at 50 °C on GGMA solutions (pre- and post-sterilization) dissolved in D_2O (5 mg/mL) at 37 °C for 1 h The degree of substitution was calculated as follows (Agibayeva et al., 2020):

$$DS\ (\%) = \frac{\frac{1}{2}I_{doublebond(methacrylate)} \Big/ \frac{1}{3}I_{CH_3(rhamnose)}}{n_{OH\ (repeating\ unit)}} \quad (1)$$

where $I_{doublebond(methacrylate)}$ is the integration of the double bond proton peak of the methacrylate groups, $I_{CH_3(rhamnose)}$ is the integration of the reference peak with the number of protons in each peak, and $n_{OH\ (repeating\ unit)}$ is the number of reactive –OH sites in the GG structure. Here, the methyl group (-CH_3) on the rhamnose ring of the GG repeating unit was used as a reference.

2.3.2. Microbiological analyses

The lyophilized GGMA powder and the PBS, used as a solvent, were microbiologically tested before and after steam sterilization (autoclave for 30 min at 1 atm at 121 °C) (Fig. 1). For this purpose, the GGMA was resuspended in PBS at 2 % w/v and was shaken and incubated in a water bath for 10 min at 37 °C, to dissolve the powder clumps. A duplicate of each sample (500 μL) was directly spread on plates of Tryptone Soya agar (Thermo Fisher Diagnostic, Basingstoke, United Kingdom), according to European (pH. Eur., X Edition, Decree, February 9th, 2020) and Italian Pharmacopoeia (Italian Official Gazette n. 79, March 25th, 2020). All plates were then incubated at 36 °C for 24, 48, and 72 h to analyse the flora growing at 36 °C in aerobic conditions, which could affect the culture. At the end of the incubation time, the plates were photographed, the colonies were counted, and the results were expressed as colony formant units (CFU) per 500 μL.

2.3.3. Rheological characterization

A rheological characterization was performed on the pre-crosslinked solutions of GGMA before and after steam sterilization, using a rheometer (Anton Paar MCR-302, Graz, Austria) equipped with a cone-plate geometry (diameter: 50 mm, angle = 1°) without adding the Ru/SPS photoinitiators. Briefly, PBS was added to the GGMA powder reaching the final concentration of 1 % and 2 % w/v, and the solutions were kept at 37 °C in the water bath until completely dissolved.

The flow curves were acquired at 25 °C at shear rates ranging from 0.1 to 1000 s^{-1} in rate-controlled mode by selecting 10 points for each decade. The viscosity was modelled as a non-Newtonian fluid according to the following power law (Denier & Dabrowski, 2004):

$$\eta = K\dot{\gamma}^{n-1} \quad (2)$$

where η is the dynamic viscosity, $\dot{\gamma}$ is the fluid shear rate, K is the consistency index and n is the flow behaviour index.

The amplitude sweep tests were carried out at 25 °C, varying the shear rate logarithmically from 0.01 % to 1000 % and setting the angular frequency at 10 s^{-1}. The temperature sweep tests were performed at a shear rate of 10 s^{-1}, varying the temperature from 15 °C to 40 °C.

2.3.4. Injectability evaluation

The injectability of GGMA solutions at concentrations of 1 % and 2 % w/v, after steam sterilization, was evaluated by performing uniaxial compression with an Instron Mechanical Testing System (model 2444, Instron, Norwood, MA, USA) equipped with ±1 kN load cell at a

compression rate of 0.64 mm·min^{-1} according to EU ISO 7886 – 1:2018 standard. A dedicated set-up was employed to vertically hold a syringe containing 3 mL of GGMA solutions, warmed at 37 °C. A 20 G stainless-steel needle (length = 36 mm) was connected to the syringe in compliance with the clinical scenario (**Fig. S1**). The force over the piston displacement was recorded. Then, the maximum force from each curve was measured, representing the injection forces required for GGMA extrusion.

2.4. Hydrogel preparation and characterization

2.4.1. Hydrogel preparation

GGMA hydrogels were fabricated by dissolving the lyophilized GGMA powder in PBS at 37 °C in a water bath to achieve a concentration of 1 % and 2 % w/v. Then, Ru (0.1, 0.2 or 0.5 × 10^{-3} M) and SPS (1, 2 or 5 × 10^{-3} M) were added to the GGMA solutions to enable the matrix photo-crosslinking in response to light. Ru/SPS as photoinitiator is featured by a high absorbence in 400–500 nm range (**Fig. S2a**). Ru and SPS were previously prepared as 20 × 10^{-3} and 200 × 10^{-3} M stock solutions in D-H_2O, respectively. Three different concentrations of Ru/SPS (0.1/1, 0.2/2 and 0.5/5 mM) were tested with both GGMA concentrations (1 % and 2 % w/v). Then, 200 μL of each pre-crosslinked GGMA solution were gently transferred into a cell crown blocking a polystyrene membrane, and inserted into a 24-wells plate. All hydrogels were cross-linked using a white LED source (RfQ – Medizintechnik, GmbH & Co) featured by a spectrum having a peak at 450 nm, as shown in **Fig. S2b**. The light was applied at a 1.5 cm distance from the hydrogel solution (intensity: 18 mW cm^{-2}) for 30, 60, or 120 s.

2.4.2. Sol fraction and swelling analysis

The sol fraction analysis was performed to determine the efficiency of the cross-linking varying the GGMA and the photoinitiator concentration at different light exposure doses. The GGMA-based hydrogels were prepared as reported in the previous section. Then, the sol fraction (%) was calculated as:

$$Sol\ fraction\ (\%) = \frac{W_{dry1} - W_{dry2}}{W_{dry1}} \times 100 \quad (3)$$

where W_{dry1} and W_{dry2} are the weights after the first and the second lyophilization steps.

Moreover, the swelling ratio (%) was calculated as follows:

$$Swelling\ ratio\ (\%) = \frac{W_{swollen}}{W_{dry2}} \times 100 \quad (4)$$

where $W_{swollen}$ and W_{dry1} are the weights before and after the second lyophilization step.

2.4.3. Compression behaviour and self-healing properties

A mechanical characterization (compression tests) was performed on the GGMA hydrogels selected after the sol fraction analysis. Here, the samples under investigation were named as GGMA2 %_0.1/1mM_60 s and GGMA2 %_0.2/2mM_30 s (the name contains information on GGMA concentration, photoinitiator concentrations and exposure time to visible light). All compression tests were carried out at room temperature and at a constant rate of 1 mm·min^{-1} until the complete breaking up of hydrogels (Trucco et al., 2021). The compressive elastic modulus, fracture stress, fracture strain, and toughness were calculated from the stress-strain curves.

For the assessment of self-healing properties induced by stress or cracks, GGMA (GGMA2 %_0.1/1mM_60 s and GGMA2 %_0.2/2mM_30 s) hydrogels were prepared, as reported in the previous section, and cut into two cylindrical halves, according to Liu et al. (Liu, Wong, Chang, & Hsu, 2021). After 10 min, the two hydrogel pieces were placed in interfacial contact in proximity to the visible cut mark, and left 6 h under moist conditions within the incubator. Then, samples were tested through a compression test, as described above.

2.4.4. Morphological analysis

The morphology of GGMA2 %_0.1/1mM_60 s and GGMA2 %_0.2/2mM_30 s hydrogel sections was characterized through SEM imaging. Cylindrical samples were cut, and the cross-sectioned surface was coated by a thin Au layer using a Mini Sputter Coater (model SC7620, Quorum, UK). An intensity of 15 mA was applied for 60 s to depose a thin film of ~5 nm in thickness under a sputter rate of 5 nm/min (at 15 mA) following the data sheet. Then, the samples were visualized through a scanning electron microscopy (SEM, Phenom XL, Thermo Fisher, USA) under high vacuum condition, by setting a beam voltage of 5 kV.

2.4.5. Diffusivity test

BSA-FITC was used to investigate the nutrient diffusion in GGMA2 %_0.1/1mM_60 s and GGMA2 %_0.2/2mM_30 s hydrogels, as already performed in our previous work (Manferdini et al., 2022). Briefly, 1 mL of the FITC-BSA solution (100 μg/mL in D-H_2O) was poured onto the upper surface of each hydrogel, and incubated for 30 min at 37 °C. Then, hydrogels were washed with PBS three times for 5 min at 37 °C to remove the residual fluorescent dye. Each hydrogel was then cut, and the cross-sectioned surface was observed with a confocal laser scanning microscope (Nikon Eclipse Ti, Tokyo, Japan) at the FITC wavelength (488 nm). Samples not incubated with the FITC-BSA were used as controls.

2.5. Biological characterization of cell-laden hydrogels

2.5.1. Cell-laden hydrogel preparation

Human chondrocytes (HCs) were thawed and maintained in culture using a company growth medium (see *Materials* section) from passages 1 to 5. At passage 5, cells were trypsinized and embedded within GGMA2 %_0.1/1mM_60 s and GGMA2 %_0.2/2mM_30 s hydrogels (density: 2 × 10^6 cells/mL). Then, the cell-laden hydrogels were photo-crosslinked with the visible LED light source. For the subsequent days in culture, the growth medium was replaced daily.

2.5.2. Live & dead assay

The viability of HCs was evaluated after 2, 7 and 14 days of culture. According to the manufacturer's instructions, the samples were washed thrice in PBS for 5 min at 37 °C and then incubated with a Live/Dead solution for 30 min at 37 °C. After staining, hydrogels were washed again three times for 5 min at 37 °C with PBS and three staked images of each sample have been taken with a confocal fluorescence microscope (Nikon Instruments Europe BW), where live cells were observed in green, while dead/necrotic ones were identified in red.

2.5.3. Metabolic activity assay

Cell metabolic activity was analysed after 2, 7 and 14 days using the PrestoBlue assay. According to the manufacturer's instructions, the samples were washed with PBS for 5 min at 37 °C and then incubated with the PrestoBlue solution diluted in HC growth medium (ratio 1:10) for 2 h Then, the supernatants were collected, and the absorbence was read at 570 nm using an automated spectrophotometric plate reader (Victor Nivo, Perkin Elmer, USA).

2.5.4. Gene expression

Total RNA was extracted from basal HCs (passage (p) from 0 to 5) cultured in monolayer on standard plastic plates and from HC-laden GGMA2 %_0.1/1mM_60 s and GGMA2 %_0.2/2mM_30 s hydrogels after 34 days of culture. Cells and cells laden hydrogels were removed from the cell culture medium and transferred in eppendof tubes. To each sample, 300 μL of TRIzol reagent were added and a mortar was used to grind the samples. Then, all samples were immediately flash frozen in liquid nitrogen (- 196 °C) and stored in a freezer at –80 °C. RNA extraction was performed as previously described (Lisignoli et al., 2014)

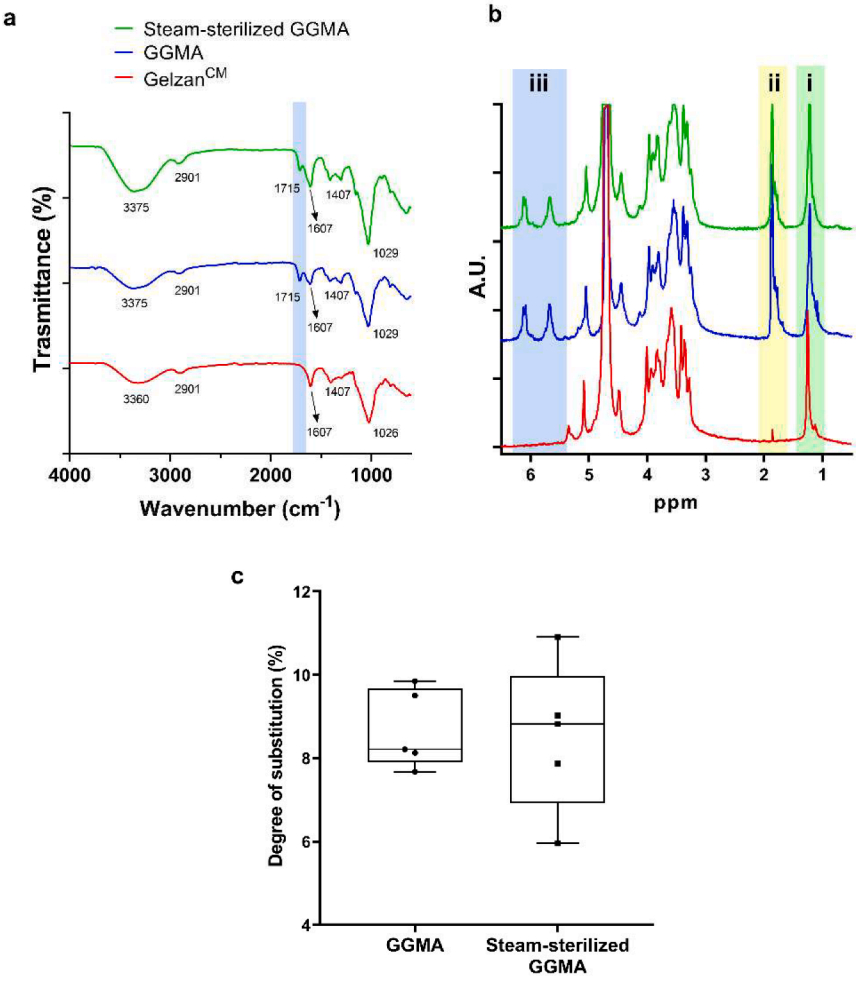

Fig. 2. (a) FT-IR analysis of GG (Gelzan^{CM}, red), GGMA before (GGMA, blue) and after steam sterilization with autoclave (Steam-sterilized GGMA, green); the blue band highlights the methacrylation group; (b) ^{1}HNMR analysis of GG (Gelzan^{CM}, red), GGMA before (GGMA, blue) and after steam sterilization with autoclave (Steam-sterilized GGMA, green); the green band (i) shows the rhamnose methyl group, the yellow (ii) and the blue (iii) bands highlight the methacrylic units; (c) comparison between the degree of substitution (%) of GGMA (before sterilization) and the steam-sterilized GGMA. Data are represented by box plots with median, minimum and maximum showing all points; $n = 5$.

and following the manufacturer's instructions. Then, the extracted RNA samples were treated with DNase I (DNA-free Kit), and RNA was quantified using a spectrophotometer (Nanodrop®, Thermo Fisher Scientific, Singapore). Reverse transcription was performed using a Super Script® Vilo™ cDNA synthesis Kit (Life Technologies, Arlsbad, CA, USA), according to the manufacturer's instructions. Real-time polymerase chain reaction (PCR) was performed with QuantStudio1 (Applied Biosystems by Thermo Fisher Scientific, Singapore) for the quantification of the following genes: collagen type II alpha chain (COL2A1), Cartilage Oligomeric Matrix Protein (COMP), marker of proliferation Ki-67 (MKI67), and collagen type I alpha 1 chain (COL1A1) (**Table. S1**). The CT value of the target gene was analysed by relative quantification using the CT value of the housekeeping gene Glyceraldeyde-3-Phosphate Dehydrogenase (GAPDH) according to the formula $2^{-\Delta Ct}$ and expressed as a percentage of the reference gene.

2.6. Statistical analysis

A normality test (D'Agostino-Pearson) was performed on all experimental data to assess data distribution. In all cases except for injection forces, data resulted having a non-normal distribution. For statistical comparisons, a parametric unpaired Student *t*-test was employed to analyse significant differences between the two groups of injection forces, while a non-parametric Kruskal–Wallis' test and Dunn's multiple comparison test were applied, to analyse significant differences between all other groups. Statistical analyses were carried out using GraphPad Prism (v 8.0.2). The significance threshold was set at 5 %.

3. Results and discussion

3.1. Characterization of GGMA powder

3.1.1. FT-IR and ^{1}HNMR

The FT-IR spectra of GG (Gelzan^{CM}), GGMA before and after the steam sterilization (steam-sterilized GGMA) were compared to assess the possible differences induced by each preparation step. The results are shown in Fig. 2a. GG, GGMA and steam-sterilized GGMA showed the typical bands of gellan gum referred to the O–H stretching at 3375 – 3360 cm^{-1}, C–H stretching at 2901 cm^{-1}, COO– asymmetric stretching at 1607 cm^{-1}, COO– symmetric stretching at 1407 cm^{-1}, and the C–O stretching at 1029 – 1026 cm^{-1} (Pereira et al., 2011; Trucco et al., 2022). The peaks due to the C = O stretching, formed as a consequence of the ester bond produced by the methacrylation procedure on one of the D-glucose residues, were clearly visible in the GGMA and the steam-sterilized GGMA, at approximately 1715 cm^{-1} (Coutinho et al., 2010; Trucco et al., 2022). This peak was still present in the autoclaved samples, highlighting that such treatment did not influence the chemical structure of the GGMA.

Table 1
Microbiological analysis on GGMA powder and PBS solution before and after the steam sterilization process. CFU = Colony forming unit. N.D. = Not Detected.

Sample	No steam sterilization	Steam sterilization with autoclave
GGMA powder	2 CFU	N.D.
PBS	N.D.	N.D.
GGMA+PBS	N.D.	N.D.

The materials were also analysed using ^{1}HNMR to investigate and quantify the GG degree of substitution induced by the methacrylation procedure, and the possible effects of the steam treatment (Fig. 2b). All spectra displayed the characteristic peak corresponding to the rhamnose methyl group methyl (–CH_3) at around 1.25 ppm (Agibayeva et al., 2020), the –CH group of glucose (4.46 ppm), the –CH group of glucuronic acid (4.71 ppm), and the –CH group of rhamnose (5.04 pp). GGMA before and after the sterilization step showed two peaks due to carbon–carbon double bond in the regions of 5.5–6.5 ppm and a peak due to the formation of a methyl group in the methacrylated material at around 1.87 ppm (Agibayeva et al., 2020; Coutinho et al., 2010; Lu, Zhao, & Fang, 2019; Silva-Correia et al., 2011; Varvarà, Tranchina, Cavallaro, & Licciardi, 2020; Xu et al., 2018).

As shown in Fig. 2c, the degree of substitution of GGMA before and after the steam sterilization did not significantly differ, and remained in the 8 – 10 % range. The degree of substitution was found within the range reported in the literature (1.2 – 11.25 %) (Coutinho et al., 2010).

Our results show that the steam sterilization did not alter the functionalization induced by GGMA methacrylation, in terms of the qualitative peak seen with the FT-IR and the quantitative NMR analysis. Steam sterilization is considered one of the pharmacopeia compendial sterilization methods, and a recognized method to sterilize materials according to the ISO 17665–1:2006. Moreover, its ease and safety of use, as well as the low cost, make it an attractive method for a broad range of applications. However, the possible effects of this treatment on the chemical properties of hydrogel are often under-investigated (Tipnis & Burgess, 2018). Its use has been recently tested with another polysaccharide, namely the alginate, comparing the influence of the treatment when sterilized in the form of solid (e.g., powder) and in solution (i.e., the polymer dissolved in water) (Lorson et al., 2020). In that study, the treatment as a powder did not alter the polymer molecular weight, while it changed when treated in the liquid form. Here, we demonstrated the possibility of treating the GGMA in the form of powder with autoclave, without varying its degree of functionalization upon methacrylation. To the best of our knowledge, no research groups reported this evidence so far, concerning GGMA.

3.1.2. Microbiological analysis

A microbiological analysis was performed to verify the sterility of the powder after steam sterilization. As shown in Table 1, a few colonies (2 CFU /500 μL) were counted in the powder alone before steam sterilization. However, no CFU were detected after the sterilization process during the whole incubation period (72 h), indicating that the sterilization procedure was effective in preventing powder contamination **Fig. S3**. reports the representative images of the agar plates incubated for 72 h at 36 °C for evaluating the flora growth. These results confirmed that this kind of sterilization might be employed to guarantee a safe use of the GGMA powder to build hydrogels in sterile conditions (thus suitable for hosting cells).

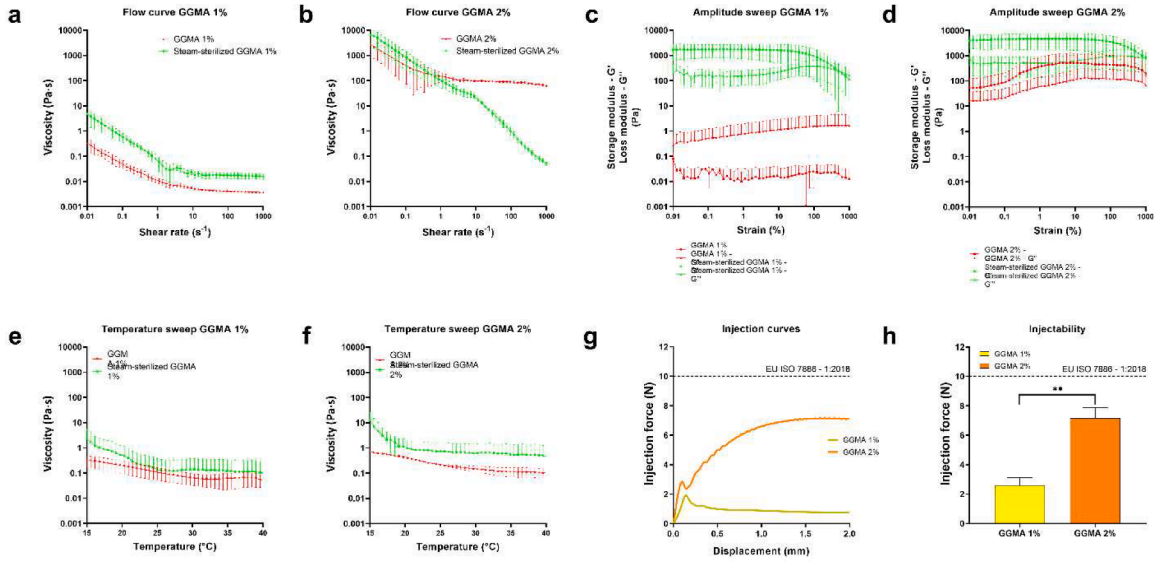

Fig. 3. Analysis of the rheological properties of GGMA at 1 % and 2 % w/v concentrations, between non-autoclaved and steam-sterilized solutions. (a-b) Flow curves (viscosity vs. shear rate); (c-d) Amplitude sweeps (storage (G') and loss (G") modulus vs. strain; (e-f) Temperature sweeps (viscosity vs. temperature). Each rheological curve represents the average value with the corresponding standard deviation; $n = 4$. (g) Force-displacement curves of GGMA at 1 % (yellow) and 2 % (red) w/v recorded during the injection tests. (h) Comparison of the maximum injection force measured to extrude the GGMA at 1 % and 2 % w/v through 20 G stainless-steel needles. Data are represented as mean ± standard deviation; $n = 10$; $^{**}p < 0.01$. The dashed line in (g) and (h) represents the injection force threshold (10 N) suitable for clinical applications according to EU ISO 7886 – 1:2018 standard.

Table 2
Rheological indexes (K, n) extracted by flow curves of GGMA 1 % and GGMA 2 %. Comparison performed only between the solutions before and after the steam sterilization with autoclave. Data are reported as mean ± standard deviation; $n = 4$; $^{*}p < 0.05$, $^{**}p < 0.01$.

	GGMA 1 %		GGMA 2 %	
	No steam sterilization	Steam sterilization	No steam sterilization	Steam sterilization
K [Pa·s^n]	0.02 ± 0.01	0.14 ± 0.02 (**)	51.64 ± 16.35	182.72 ± 84.92 (*)
n	0.64 ± 0.07	0.51 ± 0.09	0.76 ± 0.10	0.08 ± 0.04 (**)

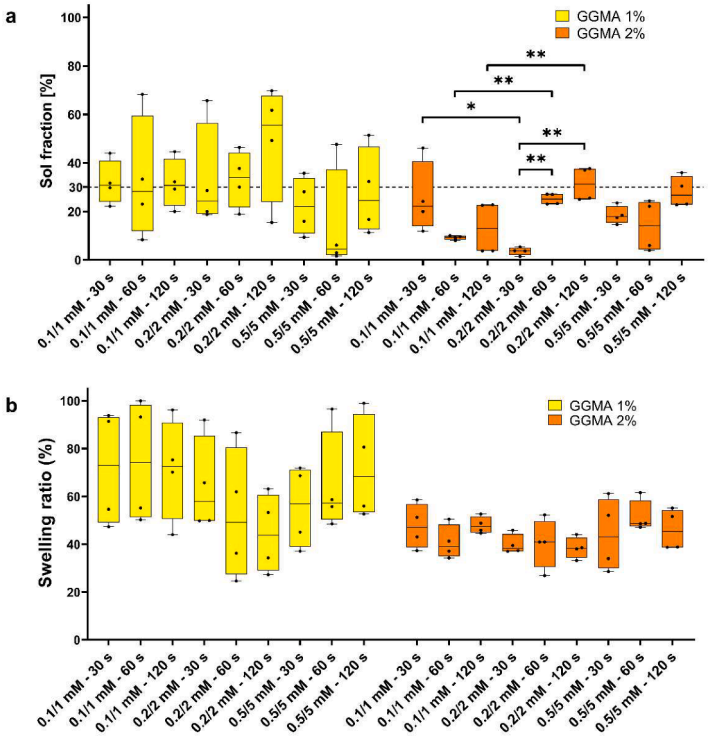

Fig. 4. Screening of the cross-linking efficiency of photopolymerized GGMA hydrogels. (a) Evaluation of sol fraction (%) of GGMA at 1 % (yellow) and 2 % (orange) w/v for each combination of Ru/SPS concentrations (0.1/1, 0.2/2 and 0.5/5 mM) and exposure times (30, 60 and 120 s). The dotted line represents the sol fraction threshold, set at 30 %. Data are represented by box plots with median, minimum and maximum showing all points; $n = 4$; $^*p < 0.05$, $^*p < 0.01$. (b) Evaluation of swelling ratio (%) of GGMA at 1 % (yellow) and 2 % (orange) w/v for each combination of Ru/SPS concentrations (0.1/1, 0.2/2 and 0.5/5 mM) and exposure times (30, 60 and 120 s). Comparison between/inside the two concentrations (1 % and/or 2 %). Data are represented by box plots with median, minimum, and maximum showing all points; $n = 4$.

3.1.3. *Rheological characterization*

The rheological properties of GGMA were investigated at different concentrations (1 % and 2 % w/v), and verifying possible differences between non-autoclaved and steam-sterilized samples. As shown in Fig. 3a,b, for both samples the viscosity decreased when the shear rate increased, indicating a shear-thinning behaviour, coherently with the findings reported by Jongprasitkul et al. (Jongprasitkul, Turunen, Parihar, & Kellomäki, 2022). However, the viscosity of steam-sterilized solutions at 2 % w/v showed a more pronounced shear-thinning behaviour, as confirmed by the steeper slope of the curve over the shear rate (Fig. 3b). The viscosity of GGMA at 2 % w/v was two orders of magnitude higher with respect to the one of GGMA at 1 % w/v. The analysis of rheological indexes (Table 2) extracted by the flow curves of Fig. 3a,b confirmed that the steam sterilization with autoclave statistically significant improved the consistency index of GGMA, while decreasing the n value. The increment in the viscosity can be attributed to the thermosensitive nature of carbohydrate polymers, a characteristic shared by many polysaccharides. Such a temperature sensitivity can have a profound impact on the material, especially during sterilization, particularly if there are no protective structural polymers (i.e., poly vinyl alcohol), as demonstrated by Leone et al. (Leone et al., 2020). The viscosity increases in carbohydrates when subjected to steam sterilization, also known as gelatinization, is primarily be due to the disruption of the native structure of the carbohydrate molecules and the reorganization of their chains. That behaviour was observed in food processing subjected to steam sterilization (e.g., sauces, soups, and other food products) (Mohamed, 2021, 2023). However, it must be highlighted that the exact effects on viscosity can vary depending on the type of carbohydrate and its initial structure, as well as the specific conditions of steam sterilization applied. Indeed, Lorson et al. reported the opposite behaviour when steam was used to sterilize alginate, observing a decrease in viscosity (Lorson et al., 2020).

To evaluate further differences in terms of viscoelastic properties, the analysis of the amplitude sweep was performed. Results show that non-autoclaved GGMA at 1 % and 2 % w/v revealed a fluid-like behaviour, highlighted by the higher loss modulus with respect to its storage modulus over the strain (Fig. 3c,d). Moreover, the cross-over point between the storage and the loss moduli did not occur in both cases within the strain range considered. Different results have been found for both steam-sterilized GGMA at 1 % and 2 % w/v, which showed a linear viscoelastic region with higher elastic modulus than their loss modulus and a well-defined cross-over point. In the state-of-the-art, similar results were obtained for a GGMA powder (derived from Gelrite®) that was dissolved at 2 % w/v in D-H2O and was previously decontaminated with UV light (Scalzone et al., 2022).

Finally, the temperature sweep tests revealed that the viscosity of all solutions remained almost constant in the range between 15 °C and 40 °C (Fig. 3e,f), suggesting the absence of a net sol-gel transition in all samples, which could alter the GGMA injectability in that operative range due to the temperature-sensitive gelation.

These results underline that the steam treatment with autoclave may improve the injectability of GGMA, by increasing its shear thinning behaviour and viscoelastic properties.

3.1.4. *Injectability evaluation*

The analysis of injectability of GGMA solutions (1 % and 2 % w/v) after steam sterilization is depicted in Fig. 3g,h. In Fig. 3g, force-displacement representative curves revealed two distinct patterns. The GGMA solution at 1 % w/v exhibited an initial peak in correspondence with the start of injection, reaching its maximum value. On the other hand, the GGMA solution at 2 % demonstrated a higher plateau force without a distinct peak, meaning that the force necessary to extrude the material at a constant rate is higher than the force required to exceed the initial friction. These trends are characteristic of force-displacement

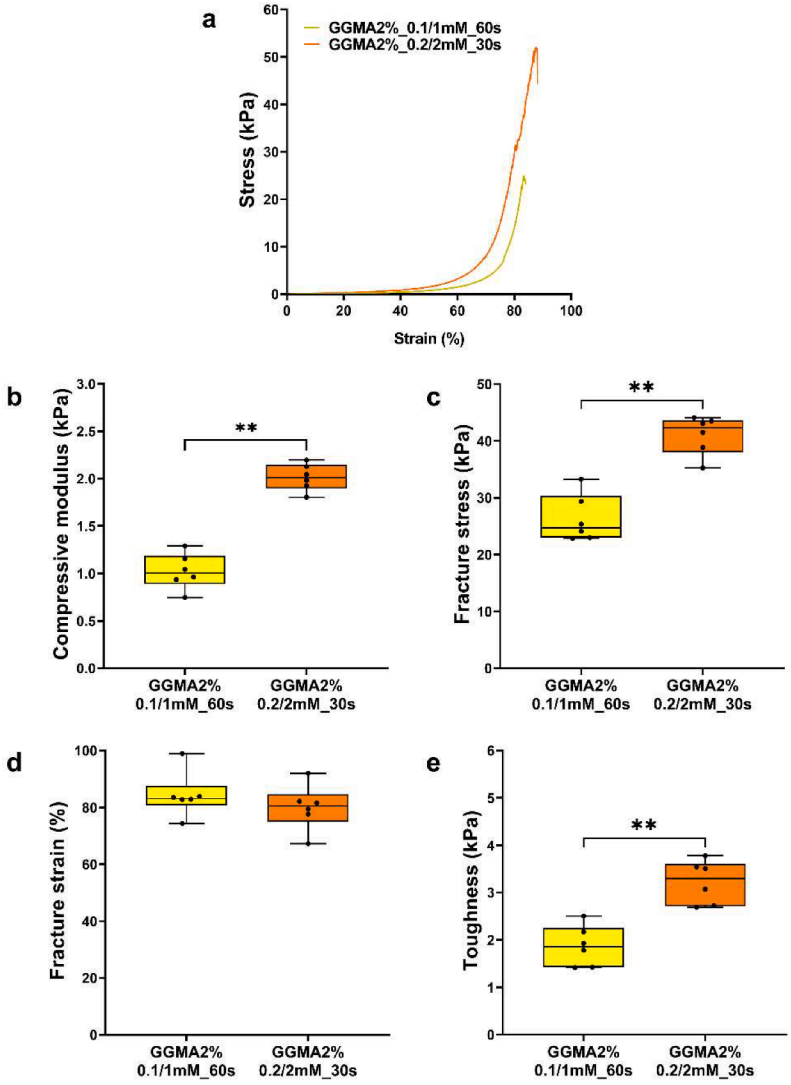

Fig. 5. Mechanical properties of GGMA2 %_0.1/1mM_60 s and GGMA2 %_0.2/2mM_30 s hydrogels. (a) Stress-strain curves, (b) compressive modulus, (c) fracture stress, (d) fracture strain and (e) toughness. Data are represented by box plots with median, minimum and maximum showing all points; $n = 6$; ** = $p < 0.01$.

curves for two scenarios: the GGMA solution at 1 % w/v resembled the behaviour of an inviscid solution passing through relatively wide needles, while the GGMA solution at 2 % w/v resembled that of a more viscous solution being ejected through narrower needles (Robinson, Hughes, Eisenstein, Grover, & Cox, 2020) even if both were injected through the same 20 G needles.

The maximum values obtained in the force-displacement curves for both solutions were subsequently extracted and illustrated in Fig. 3h. Notably, there was a statistically significant difference in the injection forces required to extrude the GGMA solutions. Specifically, the forces amounted to 2.59 ± 0.52 N and 7.18 ± 0.69 N for the 1 % and 2 % w/v GGMA concentrations, respectively. It is worth mentioning that the injection force remained below the threshold of 10 N, a criterion that determines the clinical acceptability for injectable materials, as outlined in the EN ISO 7886 – 1:2018 standard.

3.2. Sol fraction analysis

The sol fraction, defined as the weight fraction of polymer chains that are not covalently bound to the hydrogel network after photo-crosslinking, has been identified as an index to determine the visible light-mediated cross-linking efficiency of GGMA hydrogels according to the different conditions under investigation, namely GGMA concentration, photoinitiator concentration, and visible light dose. Sol fraction results (Fig. 4a) denoted that for GGMA hydrogels at 1 % w/v, only in a few cases the average sol fraction value was found below 30 %, a threshold that can be considered as the maximum one when evaluating hydrogel cross-linking efficiency. Still considering 1 % w/v GGMA, samples were also featured by a high variability. These results suggest that such formulation does not guarantee an efficient and consistent cross-linking, probably due to an excessively low concentration of GGMA, resulting in unstable hydrogels prone to dissolve in the short term.

Instead, several conditions at 2 % w/v concentration showed a sol fraction value lower than 30 %. In the case of Ru/SPS 0.1/1 mM with a cross-linking time of 60 s (GGMA2 %_0.1/1mM_60 s), the average sol fraction was 9.15 ± 0.85 %, while in the case of 0.2/2 mM with a cross-linking time of 30 s (GGMA2 %_0.2/2mM_30 s) the average sol fraction was 3.55 ± 1.6 %. All samples featured by Ru/SPS at 0.5/5 mM led to higher sol fraction values (18.47 ± 3.67 %, 13.85 ± 8.04 % and 28.01 ± 6.40 % for 30 s, 60 s and 120 s, respectively). These results suggest that using Ru/SPS up to 0.2/2 mM allowed reaching a good cross-linking efficiency, while a higher photoinitiator concentration caused instabilities in the bond formation, probably due to crosslinker saturation in absorbence (Shih, Liu, & Lin, 2017). Besides, the use of a lower concentration of photoinitiator can maximize cell viability when

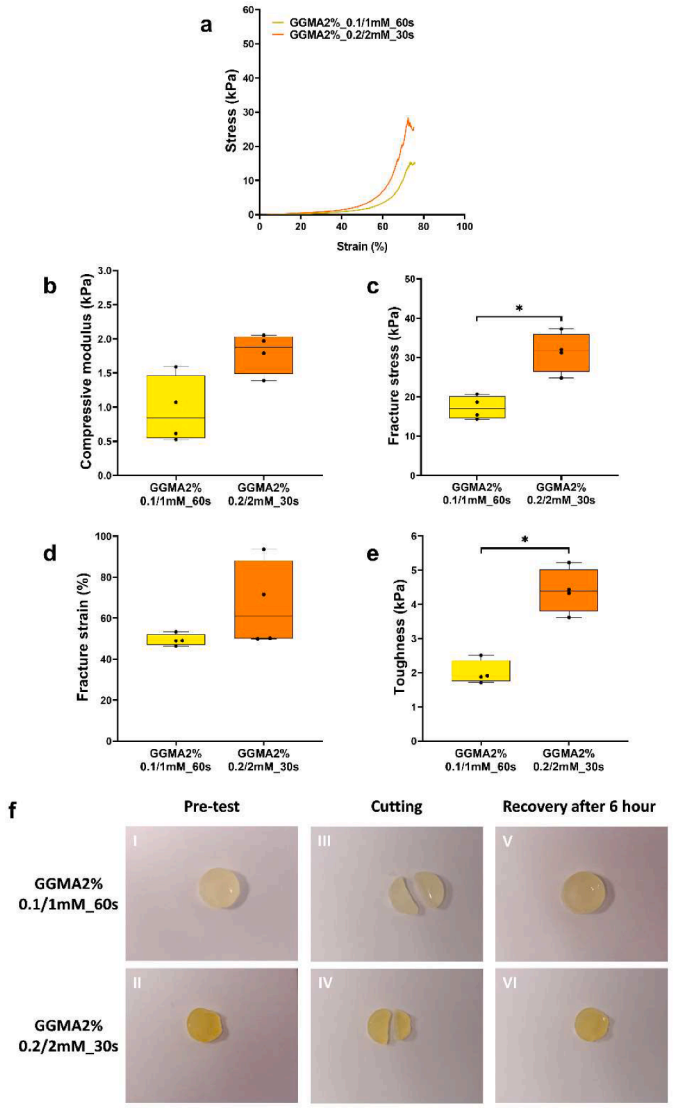

Fig. 6. Analysis of the mechanical properties of GGMA2 %_0.1/1mM_60 s and GGMA2 %_0.2/2mM_30 s hydrogels after the self-healing evaluation. (a) Stress-strain curves, (b) compressive modulus (kPa), (c) fracture stress (kPa), (d) fracture strain (%) and (e) toughness (kPa); * = $p < 0.05$. (f) Images of GGMA2 %_0.1/1MM_60S and GGMA2 %_0.2/MM_30S hydrogels before performing the cutting (I-II); images of sliced GGMA2 %_0.1/1MM_60S and GGMA2 %_0.2/MM_30S hydrogels (III-IV); Images of recovered GGMA2 %_0.1/1MM_60S and GGMA2 %_0.2/MM_30S after 6 h (V-VI). Data are represented by box plots with median, minimum and maximum showing all points; $n = 4$; * = $p < 0.05$.

embedding cells (Lim et al., 2016). Based on these results, the subsequent analyses focused on two selected formulations (GGMA2 %_0.1/1mM_60 s and GGMA2 %_0.2/2mM_30 s).

As shown in Fig. 4b, the swelling ratio trend observed for GGMA at 1 % w/v was overall higher at the one observed for 2 % w/v. The GGMA2 %_0.1/1mM_60 s and GGMA2 %_0.2/2mM_30 s formulations showed swelling ratios equal to 40.77 ± 7.01 % and 39.91 ± 4.14 %, respectively, highlighting no relevant differences in terms of water absorption between these sample types.

3.3. Mechanical characterization

The mechanical characterization of the two selected GGMA hydrogels is reported in Fig. 5. Representative stress-strain curves of both hydrogels until fracture are depicted in Fig. 5a. GGMA2 %_0.1/1mM_60 s hydrogels showed a compressive modulus equal to 1.02 ± 0.19 kPa, significantly lower than the modulus found for GGMA2 %_0.2/2mM_30 s hydrogels (2.01 ± 0.14 kPa) (Fig. 5b). Such a result was due to the higher content of Ru/SPS photoinitiator in the GGMA2 %_0.2/2mM_30 s formulation (0.2/2 mM), which may induce the formation of a higher number of chemical covalent bonds during photo-crosslinking despite the lower exposure dose. These results also suggest that the photoinitiator concentration was more impactful on the hydrogel cross-linking efficiency than the light dose provided during the cross-linking procedure. Also, applying the light for a relatively small time (60 s for GGMA2 %_0.1/1mM_60 s or 30 s for GGMA2 %_0.2/2mM_30 s), a compressive modulus in the order of kPa was obtained, a value considered suitable for hosting viable cells (Manferdini et al., 2022). Sahararo *et al.* cross-linked photosensitive GGMA-based hydrogels with a much higher exposure time (30 min) using UV light and Irgacure2959 photoinitiator, applying an intensity of 3.2 $mW \cdot cm^{-2}$ (Sahraro, Barikani, Daemi, & Baei, 2021). The hydrogels were featured by a compressive modulus of 10.70 ± 0.47 kPa. Also, Xu et al. proposed GGMA hydrogels at 1 % w/v with a Young's modulus close to 14 kPa, photo-crosslinked with UV light using a power of 15 W for 10 min (Xu et al., 2021). Apart from the achievement of stiffer matrices, the use of UV light for relatively long times (more than 10 min) may cause cell damage (Lorson et al., 2020; Vieira et al., 2020), and the need for a prolonged photo-crosslinking step would impair the translation of such materials into clinical applications (Mandal, Clegg, Anselmo, & Mitragotri, 2020). Thus, our results can be considered promising, within this perspective.

As for the compressive modulus, statistically significant differences were found in the fracture stress and the toughness between GGMA2 %_0.1/1mM_60 s and GGMA2 %_0.2/2mM_30 s hydrogels, despite no differences were found in terms of fracture strain (Fig. 5c-e). Likely, the formation of chemical covalent bonds during photo-crosslinking made the hydrogel more elastic and resistant to relatively high compressive strain values, above those the native cartilage usually supports.

We also analysed the self-healing properties of GGMA, to establish the potentiality of the hydrogels to recover from stress or cracks, which could be interesting in view of the CTE application. Indeed, self-healing may enable materials to repair themselves, by recovering mechanical properties and restoring their structure after the occurrence of defects (Hafezi, Nouri Khorasani, Zare, Esmaeely Neisiany, & Davoodi, 2021). Representative stress-strain curves of both hydrogels after the self-healing test are depicted in Fig. 6a. Both types of GGMA formulations retained the compressive modulus with respect to the bare hydrogels after the incubation period (Fig. 6b), suggesting the ability to self-repair themselves, by resisting small deformations in a similar way to when they were cross-linked (Liu et al., 2021). Indeed, the compressive modulus values are slightly less respect to the same found previously: 0.95 ± 0.48 kPa and 1.62 ± 0.44 kPa, respectively, for GGMA2 %_0.1/1mM_60 s and GGMA2 %_0.2/2mM_30 s hydrogels, and did not show any statistical differences between them (Fig. 6b). On the other hand, the fracture stress and the toughness presented statistically significant differences between GGMA2 %_0.1/1mM_60 s and GGMA2 %_0.2/2mM_30 s hydrogels (Fig. 6c,e) even though the fracture strain resulted still not different between hydrogels (Fig. 6d). About the self-healing test, explicative images of hydrogels, before and after cutting, are reported in Fig. 6f.

The self-healing nature of hydrogels may allow for retaining the structural integrity of the implant, when the material experiences cracks or structural defects (Liu et al., 2021). Indeed, because a shear-thinning when once injected (Fig. 3b), self-healing hydrogels can take the shape of the local environment, maximal interfacial contact is achieved between the hydrogel and the tissue (Uman, Dhand, & Burdick, 2020). Within the injectability suggested by rheological features, these constructs may be considered efficient cell carriers, enable minimally-invasive delivery, and provide efficient filling of irregular cavities and tissue defects (Overstreet, Dutta, Stabenfeldt, & Vernon, 2012). Self-healing hydrogels show the potential to recover from the

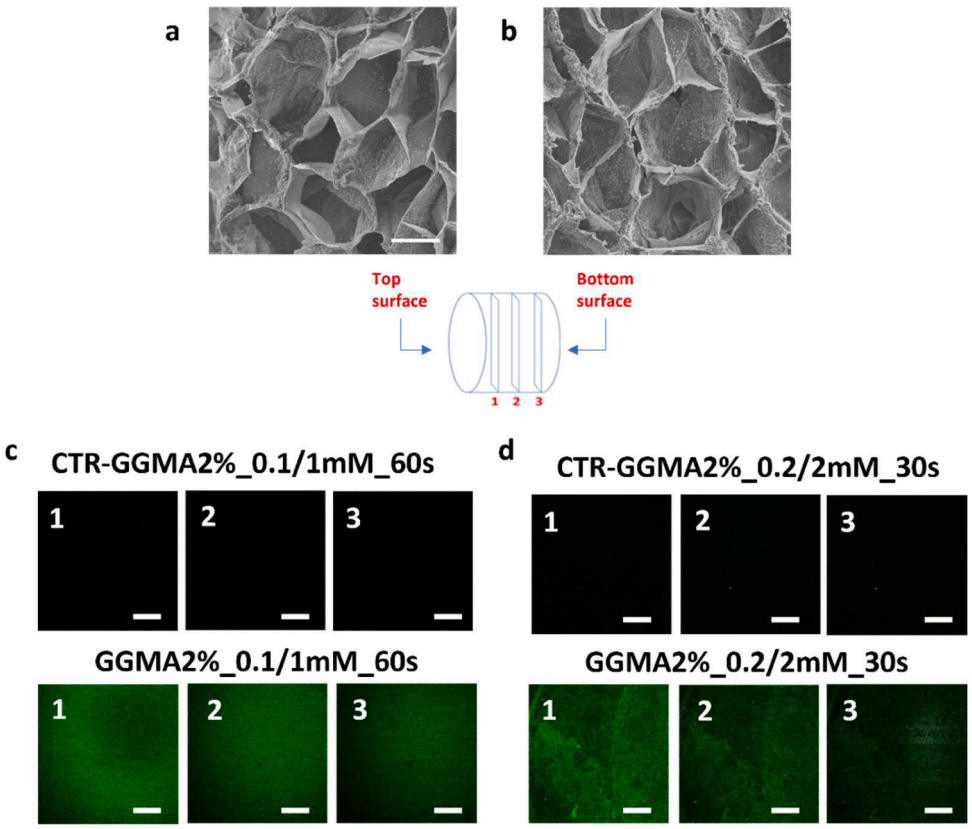

Fig. 7. SEM imaging of (a) GGMA2 %_0.1/1mM_60 s and (b) GGMA2 %_0.2/2mM_30 s hydrogels; scale bar = 50 μm. (c-d) Confocal images of the GGMA2 %_0.1/1mM_60 s and GGMA2 %_0.2/2mM_30 s hydrogels treated with BSA-FITC protein for evaluating the diffusivity throughout the hydrogels. The controls (hydrogels not exposed to BSA-FITC on the top) showed no green fluorescence. Three different planes of each hydrogel are shown (1 = top, 2 = mid, 3 = bottom) to provide an overview of the whole construct. Scale bar = 500 μm.

stress-induced formation of cracks, prolonging their lifetime, which is crucial for the implantation of engineered constructs in load-bearing zones (Uman et al., 2020).

3.4. Morphological analysis through sem imaging and diffusivity test

A morphological analysis of the selected GGMA hydrogels was performed by visualizing the hydrogel sections with SEM. Fig. 7a,b showed that both samples were featured by a porous network with open macropores in the order of 50–100 μm as diameter, which may guarantee a high degree of interconnectivity. Images also qualitatively showed that there were no marked differences between the polymeric networks.

Results of the diffusivity test are reported in Fig. 7c,d as confocal images on cross-sectioned GGMA2 %_0.1/1mM_60 s and GGMA2 %_0.2/2mM_30 s hydrogels. The controls (CTR-GGMA2 %_0.1/1mM_60 s, CTR-GGMA2 %_0.2/2m_30 s) did not exhibit relevant autofluorescence signals when not incubated with BSA-FITC throughout any level. Contrary to the controls, both GGMA-based hydrogel formulations let the protein permeation throughout all their thickness in the incubation interval. BSA-FITC has been widely used as a protein model to estimate protein diffusivity and adsorption onto the hydrogels. These results suggest that such hydrogels represent suitable platforms hosting cells due to the ability to let the nutrients diffuse within them (Manferdini et al., 2022; Yang et al., 2019).

3.5. Biological characterization

3.5.1. Cell viability and metabolic activity

The viability of HCs embedded in GGMA2 %_0.1/1mM_60 s and GGMA2 %_0.2/2mM_30 s hydrogels was investigated by L/D cell staining and visualized using confocal microscopy (Fig. 8a). The staining indicated well-distributed and viable cells (shown in green) throughout the hydrogel section on days 2, day 7 and day 14 after seeding, with only a few dead cells (shown in red). Furthermore, the evaluation of metabolic activity showed that on day 14 the amount of metabolically active cells in both GGMA hydrogels was higher with respect to the previous time points (Fig. 8b), meaning that cells were increasingly metabolically active within the hydrogels over time. On day 14, a higher activity with a statistically significant difference was observed for the GGMA2 %_0.1/1mM_60S hydrogels with respect to GGMA2 %_0.2/2mM_30S. This result reflected the different behaviour found with the L/D analysis, in which some HCs showed an elongated shape at day 14 in the GGMA2 %_0.1/1mM_60S case (zoomed images in Fig. 8a). Such a different behaviour was probably due to the lower rigidity of that formulation, which likely let cells spread and locally remodel the environment for eventually depositing of matrix throughout the material (Aprile, Whelan, Sathy, Carroll, & Kelly, 2022; Li et al., 2016; Sridhar et al., 2015).

3.5.2. Gene expression

HCs at different passages of culture for COL2A1, COL1A1, and MKI67 were analysed in terms of gene expression. As shown in **Fig. S4**, COL2A1 gradually decreased from p0 to p5. COMP, COL1A1 as MKI67 showed an up and down expression from p0 to p4, but all genes generally tended to increase at p5. HCs were encapsulated at p5 in the two different GGMA formulations and, as shown in Fig. 9, after 34 days of culture in GGMA2 %_0.1/1mM_60 s, a significant increase of typical chondrogenic COL2A1 and COMP genes expression that was associated with a decrease of fibrotic COL1A1 and proliferating MKI67 genes compared to p5. By contrast, HCs encapsulated in GGMA2 %_0.2/mM_30 s did not show an increase of COL2A1 or COMP, as found for

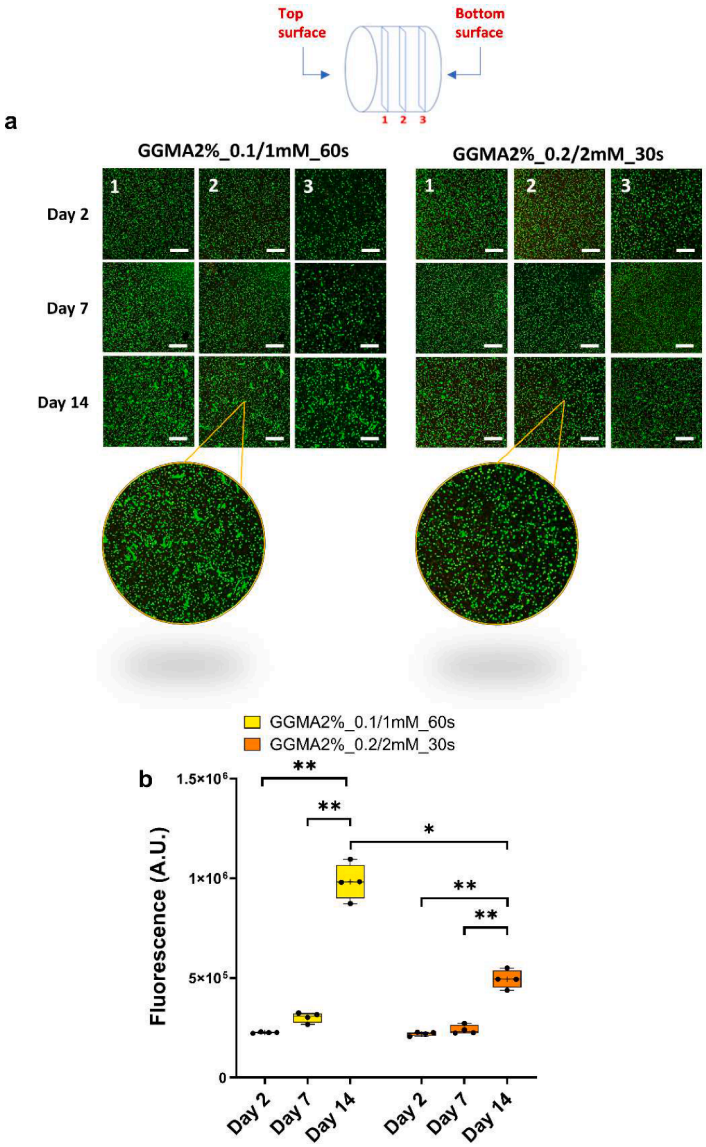

Fig. 8. (a) Confocal fluorescence images representing the outcome of viability test performed on GGMA2 %_0.1/1mM_60 s (left panel) and GGMA2 %_0.2/2mM_30 s (right panel) hydrogels embedding human chondrocytes, through the L/D assay. For each time point (day 2, 7 and 14), three different planes of the hydrogel are shown (1 = top, 2 = mid, 3 = bottom) to provide an overview of the whole construct. Live cells are coloured in green, dead/necrotic cells are coloured in red. Scale bar = 500 μm. (b) Metabolic activity of chondrocytes embedded in the GGMA2 %_0.1/1mM_60 s (yellow) and GGMA2 %_0.2/2mM_30 s (orange) hydrogels after 2, 7 and 14 days of culture. Data are represented by box plots with median, minimum and maximum showing all points; $n = 4$; * = $p < 0.05$, ** = $p < 0.01$.

GGMA2 %_0.1/1mM_60 s, but a significant decrease of COL1A1 and MKI67 is evidenced compared to P5. By comparing the two GGMA formulations, we did not evidence significant differences for all the markers analysed, although in the softer formulation the median of both COL2A1 and COMP genes have shown higher values.

The formulation GGMA 2 %_0.1/1mM_60 s assisted the redifferentiation of human chondrocytes. Similar results on COL2A1 were obtained by Pahoff et al. in GelMa-based hydrogels, even if the authors claimed a reduction in cell viability after 28 days due to the generation of free radicals during photo-crosslinking by UV light or cytotoxicity of the photoinitiator (e.g., Irgacure 2959) (Pahoff et al., 2019). These results suggested that GGMA hydrogels at the selected conditions decrease the expression of the collagen type I, which is undesired while targeting the articular cartilage, and the expression of the MKI67, a marker typical of proliferating cells. However, the softer condition (GGMA2 %_0.1/1mM_60 s) outperformed the more rigid one (GGMA2 %_0.2/2mM_30 s), demonstrating an upregulation in the expression of COL2A1 and COMP while simultaneously downregulating the expression of COL1A1. These findings support the formation of the native ECM of articular cartilage. It is widely acknowledged that the ECM comprises both collagenous components, such as COL2A1 (Wu, Korntner, Mullen, & Zeugolis, 2021) and non-collagenous proteins like COMP (Halász, Kassner, Mörgelin, & Heinegård, 2007; Maly, Andres Sastre, Farrell, Meurer, & Zaucke, 2021). These proteins play specific roles in maintaining the structural integrity of articular cartilage, including regulating collagen secretion and assembly. In cartilage tissue engineering, it is imperative avoiding or at least minimizing the formation of fibrocartilage as it can compromise ECM stability.

4. Conclusions

Methacrylated gellan gum (GGMA) represents a promising material in the cartilage tissue engineering field for restoring damaged tissue. This work demonstrated that GGMA can be sterilized through autoclave, without severely affecting the previous methacrylation procedure. Then, material rheology highlighted that the steam sterilization fostered the

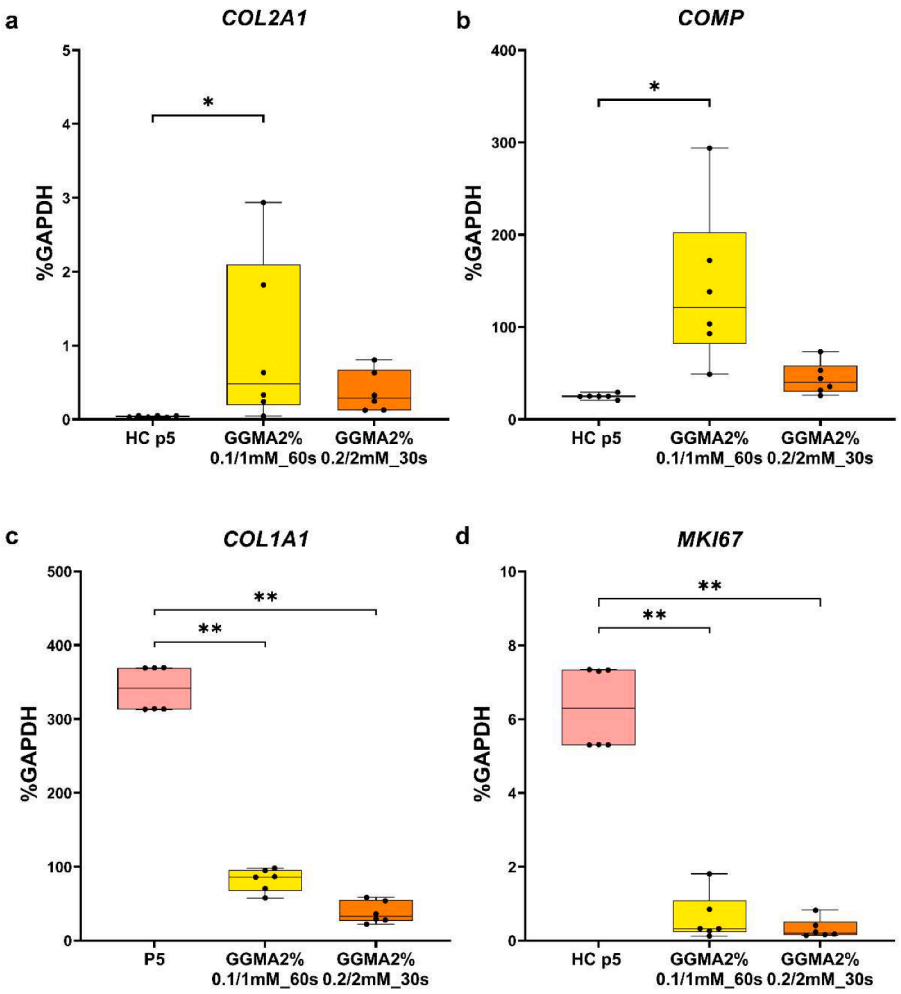

Fig. 9. Gene expression of typical [(a) COL2A1, (b) COMP], fibrotic [(c) COL1A1] and proliferating [(d) MKI67] markers, evaluated on human chondrocytes (HC) at passage 5 (p5) and on the selected GGMA formulations (GGMA2 %_0.1/1mM_60 s and GGMA2 %_0.2/2mM_30 s). The assays were performed after 34 days of culture after cell encapsulation. Data are represented by box plots with median, minimum and maximum showing all points; $n = 6$; * = $p < 0.05$, ** = $p < 0.01$.

shear-thinning and viscoelastic behaviour of GGMA solutions, increasing their potential use as injectable solutions. Indeed, both GGMA concentrations tested in this work can be injected through stainless-steel needles remaining below the force threshold outlined in the EU ISO 7886 – 1:2018 standard, and thus compliant with a possible future clinical use. From the analysis of the sol fraction of steam-sterilized GGMA hydrogels, two formulations showing the lowest values were further investigated, which differed for the photoinitiator concentration (0.1/1 mM and 0.2/2) and the exposure time (60 s and 30 s). These hydrogels showed a compressive modulus in the range of 1–2 kPa and interesting self-healing properties upon the generation of a defect. Biological analyses confirmed that human chondrocytes embedded into both hydrogel formulations exhibit high viability up to 14 days, associated with increased metabolic activity. Nonetheless, only the softer formulation (GGMA2 %_0.1/1mM_60 s, E ~1 kPa) boosted the gene expression of typical markers of the articular cartilage-like extracellular matrix (COL2A2 and COMP) on encapsulated human chondrocytes, while both formulations promoted the switching down of the fibrotic marker (COL1A1) and of the proliferating marker (MKI67).

This work demonstrated that a specific and sterile GGMA formulation obtained by photo-crosslinking after its injection may constitute a safe microenvironment for human chondrocyte encapsulation, and an instructive milieu for cells leading them to express type 2 collagen and COMP. These outcomes represent an interesting overview of the potential application of optimized GGMA in the clinical scenario to treat cartilage defects via minimally invasive procedure, opening the road for encapsulating different cell sources (i.e., stem cells) in visible light-mediated cross-linked hydrogels for cartilage tissue engineering.

Statement of significance

The paper presents an original contribution to the growing field of visible light-mediated cross-linking of hydrogels for cartilage tissue engineering. It explores the effects of steam sterilization on methacrylated gellan gum, an interesting natural polymer for cartilage tissue engineering, analysing in detail its chemical and rheological properties. The study also assesses the cross-linking efficiency of steam-sterilized materials by varying polymer and photo-initiator concentrations and exposure times to visible light. The study demonstrates that the optimized hydrogels can host human chondrocytes safely and increase the expression of articular cartilage markers. This study tackles challenges at the intersection of biomedical engineering and biomaterials science, making it of interest to researchers in these fields.

Declaration of Competing Interest

There are no conflicts to declare.

Data availability

Data will be made available on request.

Acknowledgements

This work received funding from the European Union's Horizon 2020 research and innovation program, grant agreement No 814413, project ADMAIORA (ADvanced nanocomposite MAterIals fOr in situ treatment and ultRAsound-mediated management of osteoarthritis).

The authors thank Dr. Francesca Pignatelli and Dr. Matteo Battaglini for their help in the FT-IR/^{1}HNMR data recording and confocal microscope image collection, respectively.

Supplementary materials

Supplementary material associated with this article can be found, in the online version, at doi:10.1016/j.carpta.2023.100382.

References

Agibayeva, L. E., Kaldybekov, D. B., Porfiryeva, N. N., Garipova, V. R., Mangazbayeva, R. A., & Moustafine, R. I. (2020). Gellan gum and its methacrylated derivatives as in situ gelling mucoadhesive formulations of pilocarpine: In vitro and in vivo studies. *International Journal of Pharmaceutics, 577*, Article 119093.

Aprile, P., Whelan, I. T., Sathy, B. N., Carroll, S. F., & Kelly, D. J. (2022). Soft Hydrogel Environments that Facilitate Cell Spreading and Aggregation Preferentially Support Chondrogenesis of Adult Stem Cells. *Macromolecular Bioscience, 22*(6), Article e2100365.

Armiento, A. R., Alini, M., & Stoddart, M. J. (2019). Articular fibrocartilage - Why does hyaline cartilage fail to repair? *Advanced Drug Delivery Reviews, 146*, 289–305.

Arshi, A., Petrigliano, F. A., Williams, R. J., & Jones, K. J. (2020). Stem cell treatment for knee articular cartilage defects and osteoarthritis. *Current Reviews in Musculoskeletal Medicine, 13*(1), 20–27.

Asadi, N., Alizadeh, E., Salehi, R., Khalandi, B., Davaran, S., & Akbarzadeh, A. (2018). Nanocomposite hydrogels for cartilage tissue engineering: A review. *Artificial Cells, Nanomedicine, and Biotechnology, 46*(3), 465–471.

Bacelar, A. H., Silva-Correia, J., Oliveira, J. M., & Reis, R. L. (2016). Recent progress in gellan gum hydrogels provided by functionalization strategies. *Journal of Materials Chemistry B, 4*(37), 6164–6174.

Cadet, J., Sage, E., & Douki, T. (2005). Ultraviolet radiation-mediated damage to cellular DNA. *Mutation Research/Fundamental and Molecular Mechanisms of Mutagenesis, 571*(1), 3–17.

Chimutengwende-Gordon, M., Donaldson, J., & Bentley, G. (2020). Current solutions for the treatment of chronic articular cartilage defects in the knee. *EFORT Open Rev, 5*(3), 156–163.

Coutinho, D. F., Sant, S. V., Shin, H., Oliveira, J. T., Gomes, M. E., & Neves, N. M. (2010). Modified Gellan Gum hydrogels with tunable physical and mechanical properties. *Biomaterials, 31*(29), 7494–7502.

da Silva, L. P., Jha, A. K., Correlo, V. M., Marques, A. P., Reis, R. L., & Healy, K. E. (2018). Gellan gum hydrogels with enzyme-sensitive biodegradation and endothelial cell biorecognition sites. *Advanced Healthcare Materials, 7*(5), Article 1700686.

Denier, J. P., & Dabrowski, P. P. (2004). On the boundary–layer equations for power–law fluids. *Proceedings of the Royal Society of London. Series A: Mathematical, Physical and Engineering Sciences, 460*(2051), 3143–3158.

Hafezi, M., Nouri Khorasani, S., Zare, M., Esmaeely Neisiany, R., & Davoodi, P. (2021). Advanced hydrogels for cartilage tissue engineering: Recent progress and future directions. *Polymers (Basel), 13*(23), 4199.

Halász, K., Kassner, A., Mörgelin, M., & Heinegård, D. (2007). Comp acts as a catalyst in collagen fibrillogenesis *. *Journal of Biological Chemistry, 282*(43), 31166–31173.

Huang, J., Liu, F., Su, H., Xiong, J., Yang, L., Xia, J., et al. (2022). Advanced nanocomposite hydrogels for cartilage tissue engineering. *Gels (Basel, Switzerland), 8*(2), 138.

Jongprasitkul, H., Turunen, S., Parihar, V. S., & Kellomäki, M. (2022). Two-step crosslinking to enhance the printability of methacrylated gellan gum biomaterial ink for extrusion-based 3D bioprinting. *Bioprinting, 25*, e00185.

Kanca, Y., & Özkahraman, B. (2023). An investigation on tribological behavior of methacrylated κ-carrageenan and gellan gum hydrogels as a candidate for chondral repair. *Journal of Biomaterials Applications, 37*(7), 1271–1285.

Kim, T.-R., Kim, M.-S., Goh, S. T., Lee, S. J., Kim, H. Y., Yoon, S.-Y., et al. (2019). Evaluation of structural and mechanical properties of porous artificial bone scaffolds fabricated via advanced tba-based freeze-gel casting technique. *Applied Sciences, 9*(9), 1965.

Kwon, H., Brown, W. E., Lee, C. A., Wang, D., Paschos, N., & Hu, J. C. (2019). Surgical and tissue engineering strategies for articular cartilage and meniscus repair. *Nat Rev Rheumatol, 15*(9), 550–570.

Lee, S., Choi, J. H., Park, A., Rim, M., Youn, J., Lee, W., et al. (2020a). Advanced gellan gum-based glycol chitosan hydrogel for cartilage tissue engineering biomaterial. *International Journal of Biological Macromolecules, 158*, 452–460.

Lee, C., O'Connell, C. D., Onofrillo, C., Choong, P. F. M., Di Bella, C., & Duchi, S. (2020b). Human articular cartilage repair: Sources and detection of cytotoxicity and genotoxicity in photo-crosslinkable hydrogel bioscaffolds. *Stem Cells Translational Medicine, 9*(3), 302–315.

Learmonth, D. A., Costa, P. M., Veloso, T. R., Cunha, C. B., Cautela, M. P., Correia, C., et al. (2020). Synthesis and biological evaluation of a bioinspired, tissue-adhesive gellan gum-based hydrogel designed for minimally invasive delivery and retention of chondrogenic cells. *Biomaterials Science, 8*(13), 3697–3711.

Leone, G., Consumi, M., Pepi, S., Pardini, A., Bonechi, C., Tamasi, G., et al. (2020). Enriched gellan gum hydrogel as visco-supplement. *Carbohydrate Polymers, 227*, Article 115347.

Li, X., Chen, S., Li, J., Wang, X., Zhang, J., Kawazoe, N., et al. (2016). 3D culture of chondrocytes in gelatin hydrogels with different stiffness. *Polymers, 8*(8), 269.

Lim, K. S., Schon, B. S., Mekhileri, N. V., Brown, G. C. J., Chia, C. M., Prabakar, S., et al. (2016). New visible-light photoinitiating system for improved print fidelity in gelatin-based bioinks. *ACS Biomaterials Science & Engineering, 2*(10), 1752–1762.

Lim, K. S., Klotz, B. J., Lindberg, G. C. J., Melchels, F. P. W., Hooper, G. J., Malda, J., et al. (2019). Visible Light Cross-Linking of Gelatin Hydrogels Offers an Enhanced Cell Microenvironment with Improved Light Penetration Depth. *Macromolecular Bioscience, 19*(6), Article 1900098.

Lisignoli, G., Manferdini, C., Lambertini, E., Zini, N., Angelozzi, M., Gabusi, E., et al. (2014). Chondrogenic potential of slug-depleted human mesenchymal stem cells. *Tissue Engineering Part A, 20*(19–20), 2795–2805.

Liu, Y., Wong, C.-W., Chang, S.-W., & Hsu, S.-h. (2021). An injectable, self-healing phenol-functionalized chitosan hydrogel with fast gelling property and visible light-crosslinking capability for 3D printing. *Acta Biomaterialia, 122*, 211–219.

Lorson, T., Ruopp, M., Nadernezhad, A., Eiber, J., Vogel, U., Jungst, T., et al. (2020). Sterilization methods and their influence on physicochemical properties and bioprinting of alginate as a bioink component. *ACS Omega, 5*(12), 6481–6486.

Lu, Y., Zhao, X., & Fang, S. (2019). Characterization, antimicrobial properties and coatings application of gellan gum oxidized with hydrogen peroxide. *Foods, 8*(1), 31.

Maly, K., Andres Sastre, E., Farrell, E., Meurer, A., & Zaucke, F. (2021). COMP and TSP-4: Functional Roles in Articular Cartilage and Relevance in Osteoarthritis. *International Journal of Molecular Sciences, 22*(5), 2242.

Mandal, A., Clegg, J. R., Anselmo, A. C., & Mitragotri, S. (2020). Hydrogels in the clinic. *Bioengineering & Translational Medicine, 5*(2), e10158. https://doi.org/10.1002/btm2.10158

Manferdini, C., Trucco, D., Saleh, Y., Gabusi, E., Dolzani, P., Lenzi, E., et al. (2022). RGD-functionalized hydrogel supports the chondrogenic commitment of adipose mesenchymal stromal cells. *Gels (Basel, Switzerland), 8*(6), 382.

Mohamed, I. O. (2021). Effects of processing and additives on starch physicochemical and digestibility properties. *Carbohydrate Polymer Technologies and Applications, 2*, Article 100039.

Mohamed, I. O. (2023). Interaction of starch with some food macromolecules during the extrusion process and its effect on modulating physicochemical and digestible properties. A review. *Carbohydrate Polymer Technologies and Applications, 5*, Article 100294.

Oliveira, J. T., Santos, T. C., Martins, L., Picciochi, R., Marques, A. P., & Castro, A. G. (2010a). Gellan gum injectable hydrogels for cartilage tissue engineering applications: In vitro studies and preliminary in vivo evaluation. *Tissue Engineering Part A, 16*(1), 343–353.

Oliveira, J. T., Martins, L., Picciochi, R., Malafaya, P. B., Sousa, R. A., & Neves, N. M. (2010b). Gellan gum: A new biomaterial for cartilage tissue engineering applications. *Journal of Biomedical Materials Research Part A, 93A*(3), 852–863.

Oliveira, I. M., Gonçalves, C., Shin, M. E., Lee, S., Reis, R. L., Khang, G., et al. (2021). Enzymatically crosslinked tyramine-gellan gum hydrogels as drug delivery system for rheumatoid arthritis treatment. *Drug Delivery and Translational Research, 11*(3), 1288–1300.

Overstreet, D. J., Dutta, D., Stabenfeldt, S. E., & Vernon, B. L. (2012). Injectable hydrogels. *Journal of Polymer Science Part B: Polymer Physics, 50*(13), 881–903.

Pahoff, S., Meinert, C., Bas, O., Nguyen, L., Klein, T. J., & Hutmacher, D. W. (2019). Effect of gelatin source and photoinitiator type on chondrocyte redifferentiation in gelatin methacryloyl-based tissue-engineered cartilage constructs. *Journal of Materials Chemistry B, 7*(10), 1761–1772.

Pereira, D. R., Silva-Correia, J., Caridade, S. G., Oliveira, J. T., Sousa, R. A., & Salgado, A. J. (2011). Development of gellan gum-based microparticles/hydrogel matrices for application in the intervertebral disc regeneration. *Tissue Eng Part C Methods, 17*(10), 961–972.

Rizwan, M., Chan, S. W., Comeau, P. A., Willett, T. L., & Yim, E. K. F. (2020). Effect of sterilization treatment on mechanical properties, biodegradation, bioactivity and printability of GelMA hydrogels. *Biomedical Materials, 15*(6), Article 065017.

Robinson, T. E., Hughes, E. A. B., Eisenstein, N. M., Grover, L. M., & Cox, S. C. (2020). The Quantification of injectability by mechanical testing. *JoVE*, (159), e61417. https://doi.org/10.3791/61417

Sahraro, M., Barikani, M., Daemi, H., & Baei, P. (2021). Anti-fatigue, highly resilient photocrosslinkable gellan gum hydrogels reinforced by flexible nanoparticulate polyurethane multi-crosslinkers. *International Journal of Biological Macromolecules, 183*, 831–838.

Scalzone, A., Cerqueni, G., Bonifacio, M. A., Pistillo, M., Cometa, S., & Belmonte, M. M. (2022). Valuable effect of Manuka Honey in increasing the printability and chondrogenic potential of a naturally derived bioink. *Materials Today Bio, 14*, Article 100287.

Shih, H., Liu, H.-Y., & Lin, C.-C. (2017). Improving gelation efficiency and cytocompatibility of visible light polymerized thiol-norbornene hydrogels via addition of soluble tyrosine. *Biomaterials Science, 5*(3), 589–599.

Silva-Correia, J., Oliveira, J. M., Caridade, S. G., Oliveira, J. T., Sousa, R. A., & Mano, J. F. (2011). Gellan gum-based hydrogels for intervertebral disc tissue-engineering applications. *Journal of Tissue Engineering and Regenerative Medicine, 5*(6), e97–e107.

Silva-Correia, J., Zavan, B., Vindigni, V., Silva, T. H., Oliveira, J. M., Abatangelo, G., et al. (2013). Biocompatibility evaluation of ionic- and photo-crosslinked

methacrylated gellan gum hydrogels: In vitro and in vivo study. *Advanced Healthcare Materials, 2*(4), 568–575.
Sridhar, B. V., Dailing, E. A., Brock, J. L., Stansbury, J. W., Randolph, M. A., & Anseth, K. S. (2015). A biosynthetic scaffold that facilitates chondrocyte-mediated degradation and promotes articular cartilage extracellular matrix deposition. *Regenerative Engineering and Translational Medicine, 1*(1), 11–21.
Su, W. Y., Chen, Y. C., & Lin, F. H. (2010). Injectable oxidized hyaluronic acid/adipic acid dihydrazide hydrogel for nucleus pulposus regeneration. *Acta Biomaterialia, 6*(8), 3044–3055.
Tipnis, N. P., & Burgess, D. J. (2018). Sterilization of implantable polymer-based medical devices: A review. *International Journal of Pharmaceutics, 544*(2), 455–460.
Trucco, D., Vannozzi, L., Teblum, E., Telkhozhayeva, M., Nessim, G. D., Affatato, S., et al. (2021). Graphene oxide-doped gellan gum–pegda bilayered hydrogel mimicking the mechanical and lubrication properties of articular cartilage. *Advanced Healthcare Materials, 10*(7), Article 2001434.
Trucco, D., Riacci, L., Vannozzi, L., Manferdini, C., Arrico, L., Gabusi, E., et al. (2022). Primers for the Adhesion of Gellan Gum-Based Hydrogels to the Cartilage: A Comparative Study. *Macromolecular Bioscience, 22*(10), Article 2200096.
Uman, S., Dhand, A., & Burdick, J. A. (2020). Recent advances in shear-thinning and self-healing hydrogels for biomedical applications. *Journal of Applied Polymer Science, 137*(25), 48668.
Varvarà, P., Tranchina, L., Cavallaro, G., & Licciardi, M. (2020). Preparation and characterization of gold nanorods coated with gellan gum and lipoic acid. *Applied Sciences, 10*.
Vieira, S., Strymecka, P., Stanaszek, L., Silva-Correia, J., Drela, K., Fiedorowicz, M., et al. (2020). Methacrylated gellan gum and hyaluronic acid hydrogel blends for image-guided neurointerventions. *Journal of Materials Chemistry B, 8*(27), 5928–5937.
Vilela, C. A., Correia, C., da Silva Morais, A., Santos, T. C., Gertrudes, A. C., & Moreira, E. S. (2018). In vitro and in vivo performance of methacrylated gellan gum hydrogel formulations for cartilage repair*. *Journal of Biomedical Materials Research Part A, 106*(7), 1987–1996.
Wang, Y., Yuan, M., Guo, Q.-Y., Lu, S.-B., & Peng, J. (2015). Mesenchymal stem cells for treating articular cartilage defects and osteoarthritis. *Cell Transplantation, 24*(9), 1661–1678.
Wei, W., Ma, Y., Yao, X., Zhou, W., Wang, X., Li, C., et al. (2021). Advanced hydrogels for the repair of cartilage defects and regeneration. *Bioactive Materials, 6*(4), 998–1011.
Wu, Z., Korntner, S. H., Mullen, A. M., & Zeugolis, D. I. (2021). Collagen type II: From biosynthesis to advanced biomaterials for cartilage engineering. *Biomaterials and Biosystems, 4*, Article 100030.
Xu, Z., Li, Z., Jiang, S., & Bratlie, K. M. (2018). Chemically modified gellan gum hydrogels with tunable properties for use as tissue engineering scaffolds. *ACS Omega, 3*(6), 6998–7007.
Xu, Z., Zhang, L., Bentil, S. A., & Bratlie, K. M. (2021). Gellan gum-gelatin viscoelastic hydrogels as scaffolds to promote fibroblast differentiation. *Materials Science and Engineering: C, 129*, Article 112370.
Yang, J., Li, Y., Liu, Y., Li, D., Zhang, L., Wang, Q., et al. (2019). Influence of hydrogel network microstructures on mesenchymal stem cell chondrogenesis in vitro and in vivo. *Acta Biomaterialia, 91*, 159–172.
Zhang, Y., Xu, J., Qu, Y., Xi, X., & Yang, J. (2014). Gelcasting of alumina suspension using gellan gum as gelling agent. *Ceramics International, 40*(4), 5715–5721.
Zheng, Z., Eglin, D., Alini, M., Richards, G. R., Qin, L., & Lai, Y. (2021). Visible light-induced 3d bioprinting technologies and corresponding bioink materials for tissue engineering: A review. *Engineering, 7*(7), 966–978.